

Freezing of simple fluids in microporous activated carbon fibers: Comparison of simulation and experiment

Ravi Radhakrishnan and Keith E. Gubbins

North Carolina State University, 113 Riddick Labs, Raleigh, North Carolina 27695-7905

Ayumi Watanabe and Katsumi Kaneko

Department of Chemistry, Faculty of Science, Chiba University, Yayoi 1-33, Inage, Chiba 263-8522, Japan

(Received 13 July 1999; accepted 23 August 1999)

We study the freezing of CCl_4 in microporous activated carbon fibers (ACF), using Monte Carlo simulation and differential scanning calorimetry (DSC). Microporous activated carbon fibers are well characterized porous materials, having slit-shaped pores due to the voids formed between graphitic basal planes. They serve as highly attractive adsorbents for simple nonpolar molecules, the adsorbent-adsorbate interaction being mostly dispersive (of the van der Waals-type). Recent molecular simulation studies have predicted an *upward shift* in the freezing temperature ($\Delta T_f = T_{f,\text{pore}} - T_{f,\text{bulk}} > 0$) for simple fluids confined in such highly attractive carbon slit pores. Our DSC experiments verify these predictions about the *increase* in T_f . The results also indicate significant deviation from the prediction of ΔT_f based on the Gibbs-Thomson equation (simple capillary theory). We employ a recently developed free energy method to calculate the exact freezing temperature in these confined systems using molecular simulation, in order to address the failure of the simple capillary theory. © 1999 American Institute of Physics. [S0021-9606(99)50943-4]

I. INTRODUCTION

Improved understanding of confinement effects on freezing are essential in areas relating to lubrication, adhesion, fabrication of nanomaterials and nanotribology. In addition, these studies can provide insight into mechanisms involved in frost heaving and distribution of pollutants in soils. Freezing in porous media has been widely employed in the characterization of porous materials. In the method termed thermoporometry,¹ the shift in freezing temperature of water is determined, and the pore size distribution is inferred from a thermodynamic analysis which is analogous to the use of Kelvin's equation for capillary condensation. While this is rigorous for the characterization of materials having large pores, such an analysis breaks down in the case of micropores, as the limit of small and inhomogeneous systems demand a more rigorous statistical mechanical treatment.

Experiments on freezing that have used porous silica glass as the confinement medium have always resulted in a decrease in the freezing temperature, T_f , as compared to the bulk.²⁻¹⁷ Freezing of oxygen in sol-gel glasses was studied by Warnock and co-workers² by a subpicosecond optical technique. In this method, birefringence in optical pump pulses caused by the rotational motion of the molecules in the liquid was used to measure the subsequent molecular orientational relaxation time. A change in the value of the relaxation time provided an indication of the freezing temperature. The freezing temperature in the confined system was always depressed as compared to the bulk; the shift was larger for smaller pores, and as large as 10 K for the smallest (20 nm) pore. Unruh and co-workers⁸ examined the melting behavior of indium metal in porous silica glasses by differential scanning calorimetry (DSC) measurements, and reported a large depression in melting point due to confine-

ment. Sliwiska-Bartkowiak and co-workers determined the melting/freezing transition for a dipolar fluid, nitrobenzene confined in controlled pore glass of different pore sizes, using DSC and dielectric relaxation spectroscopy.¹⁷ The results from both experiments were in good agreement.

A classical thermodynamic argument based on simple capillary theory determines the freezing temperature as the point at which the chemical potential of the solid core inside the pore equals that of the surrounding fluid (for example, see Ref. 18),

$$\frac{\Delta T_f}{T_{fb}} = -2 \frac{(\gamma_{ws} - \gamma_{wl}) \nu}{H \lambda_{fb}}, \quad (1)$$

where T_{fb} is the bulk freezing temperature, γ_{ws} and γ_{wl} are the corresponding wall-solid and wall-fluid surface tensions, ν is the molar volume of the liquid, λ_{fb} is the latent heat of melting in the bulk and H is the pore width. Equation (1) is sometimes referred to as the Gibbs-Thomson equation. The sign of $\Delta T_f = T_f - T_{fb}$ depends on whether γ_{ws} is greater or less than γ_{wl} . The observed depression in the melting temperatures varied linearly as $1/H$ in the above mentioned studies, and were thus consistent with Eq. (1) down to pore sizes as low as 6 nm.

Experimental studies that probe the structure of the confined phases using x-ray diffraction techniques, NMR, and other spectroscopic methods have been reported. Overloop and Van Gervan¹⁵ studied freezing of water in porous silica using the NMR method, and found that, in the confined solid phase, up to three molecular layers adjacent to the pore wall (which they term "bound water") have a structure that is different from the crystal phase and from that of the free liquid. The rest of the water molecules in the pore interior were in the form of cubic ice (I_c) and the freezing tempera-

tures were consistent with Eq. (1). The study also suggested a distribution of the molecular correlation times associated with translation and rotation in the bound water phase, with values lying in between those typical of liquid and crystal phases. Morishige and co-workers^{13,14} used x-ray diffraction to study water in siliceous MCM-41, for a range of average pore sizes, and also confirmed the existence of a disordered layer of water molecules near the pore wall, with the inner region being the I_c phase. In a recent study, Booth and Strange¹⁶ examined the melting of cyclohexane in porous silica using the NMR technique. The melting temperature was below the bulk melting point, and in the confined solid phase, there were two distinct components of the transverse relaxation time. The short component (15–30 μ s, comparable to the crystal phase in the bulk) was attributed to the crystal phase in the interior of the pore, and the long component was attributed to a liquidlike contact layer. Further lowering the temperature led to the freezing of the surface (contact) layer as well. In the dielectric relaxation spectroscopy study of nitrobenzene in controlled pore glass,¹⁷ quantitative estimates of the rotational relaxation time in the fluid and crystal phases were made by fitting the complex permittivity $\epsilon^* = \epsilon'(\omega) - i\epsilon''(\omega)$ measurements to the Debye dispersion equation.^{19,20} In addition to the liquid and crystal phase relaxation, a third relaxation component was observed, that supported the existence of a contact layer with dynamic properties that were more liquid like, but different from the inner layers as found in the previous studies. The linear behavior between ΔT_f and $1/H$ predicted by the Gibbs–Thomson equation was observed for pore widths down to about 8 nm, but broke down for smaller pores. This can be attributed to the fact that the presence of a contact layer with different dynamic and structural properties compared to the pore-interior is not accounted for. The effect of the contact layer on the freezing of the inner layers of the pore is expected to increase as the pore width decreases. In addition, for small and inhomogeneous systems, the concept of surface tension is not well defined, so that the Gibbs–Thomson equation cannot hold.

In view of the large body of experimental evidence for a decrease in the freezing temperature due to confinement, it is tempting to assume that a decrease always occurs. However, in a subsequent molecular simulation study of freezing of simple fluids in slit pores, Miyahara and Gubbins²¹ showed that T_f was strongly affected by the strength of the attractive forces between the fluid molecules and the pore walls. For repulsive or weakly attractive potentials, the shift in the freezing temperature ΔT_f was negative. For strongly attracting walls such as carbons, an *increase* in T_f was observed. Moreover, the increase in T_f was predicted to be larger for slit than cylindrical pores.²² Suzuki *et al.* studied the mechanism of pore filling for Lennard-Jones (LJ) CCl_4 in graphitic micropores using GCMC simulation, and found radial distribution functions in the confined phase similar to the plastic crystalline form of bulk CCl_4 at a temperature that was 50 K above the bulk freezing temperature.²³ The predictions of Miyahara and Gubbins²¹ were confirmed by free energy studies in which the thermodynamic freezing temperature in confined systems was determined; these studies established

TABLE I. Summary of pore widths.

Pore type	H/nm experiment	H/nm simulation	No. of layers
Micropores			
...	...	0.94	1
P5	1.09	...	1–2
P10	1.20	...	1–2
P20	1.44	1.44	2
...	1.74	1.74	3
...	...	1.93	3
Mesopores			
...	...	2.44	4
...	...	2.93	5
...	...	3.87	7
...	...	7.25	14

the order of the phase transition.^{24,25} Dominguez *et al.*²⁴ used thermodynamic integration²⁶ to calculate the free energy of the solid and fluid phases in the pore. This method involves a numerical integration of the Gibbs free energy starting from a known reference phase (the Einstein crystal for the solid phase and the ideal gas for the liquid phase) to the state point of interest. However, this study was limited to confined systems with repulsive or weakly attractive wall–fluid potentials. For the more ubiquitous case of a wall–fluid potential that is moderately or strongly attractive, this method breaks down. This is because the adsorbed molecules adjacent to the pore–wall (the contact layer) freeze before the adsorbed molecules in the interior of the pore. This makes it impossible to find a reversible path from the ideal gas phase to the fluid phase, since any such path runs into a first order transition corresponding to the freezing of the contact layer. Radhakrishnan and Gubbins²⁵ used a method based on an order parameter formulation^{27–29} to calculate the free energy that circumvents the problem encountered by using thermodynamic integration. The authors calculated the grand free energy for the freezing of LJ methane between strongly attractive carbon slit pores, as well as for a purely repulsive hard wall pore. They calculated the exact freezing temperature for the contact layers as well as for the inner layers; the study also established that both the transitions were first order.

In this paper, we describe DSC experiments on the freezing of CCl_4 in activated carbon fibers (ACF's) that provide clear evidence of an *increase* in freezing temperature due to confinement, verifying the predictions of the recent simulation studies. We compare the experimental results, with results obtained using the free energy method based on order parameter formulation and Monte Carlo simulation. The DSC experiments were carried out at Chiba University, Japan and the computer simulations were done at North Carolina State University, USA.

II. METHODS

A. Experimental method

Pitch-based activated carbon fibers of different pore widths (P5, P10, and P20, see Table I) in the micropore

TABLE II. Physical properties of CCl₄.

Property	Real CCl ₄	LJ-CCl ₄
T_m (at 1 atm)	251.8 K	252 K
ρ_l	1.59 g/cm ³	1.55 g/cm ³
Crystal type	Rhombohedral	fcc
λ_f	16.1 J/g	21.3 J/g

region were used as adsorbent materials. The pore width H reported throughout this paper is the distance between the planes through the carbon nuclei in the first atomic layer of each of the opposing walls. The micropore volume, specific surface area, and the average slit pore width were determined by high resolution N₂ adsorption measurements at 77 K.³⁰ CCl₄ was adsorbed on dry ACF samples at 303 K from a gas phase at the saturated vapor pressure. The DSC scans were performed at temperature scanning rates of 5.0–1.0 K min⁻¹ using a MAC Science, DSC3100 calorimeter. The freezing and melting temperatures were measured by identifying the peak positions in the DSC scan relative to the background, and the enthalpies of the phase change were calculated from the peak areas.

B. Simulation method

1. Potential models

The interaction between the adsorbed fluid molecules is modeled using the Lennard-Jones (12,6) potential with size and energy parameters chosen to describe CCl₄. The LJ parameters were fitted to the bulk properties at solid–liquid coexistence, and are

$$\sigma_{ff} = 0.514 \text{ nm}, \quad \epsilon_{ff}/k_B = 366 \text{ K}.$$

The above parameters predict the correct melting temperature (T_m) and liquid density (ρ_l) at coexistence, at a pressure of 1 atm. However, these parameters fail to predict the correct crystal structure; the LJ crystal is fcc, while real CCl₄ freezes into a rhombohedral phase. As a result, the latent heat of melting, λ_f , is not given accurately by this model. The properties of real CCl₄ and LJ-CCl₄ are compared in Table II.

We model activated carbon fibers as regular slitlike graphite pores. For the fluid–wall interaction, we use the integrated “10-4-3” Steele potential^{31,32} that corresponds to a smooth wall,

$$\phi_{fw}(z) = 2\pi\rho_w\epsilon_{fw}\sigma_{fw}^2\Delta\left[\frac{2}{5}\left(\frac{\sigma_{fw}}{z}\right)^{10} - \left(\frac{\sigma_{fw}}{z}\right)^4 - \left(\frac{\sigma_{fw}^4}{3\Delta(z+0.61\Delta)^3}\right)\right]. \quad (2)$$

The potential parameters for the graphite wall were taken from Refs. 31 and 32,

$$\begin{aligned} \sigma_{ww} &= 0.340 \text{ nm}, & \epsilon_{ww}/k_B &= 28.0 \text{ K}, \\ \rho_w &= 114 \text{ nm}^{-3}, & \Delta &= 0.335 \text{ nm}, \\ \sigma_{fw} &= (\sigma_{ff} + \sigma_{ww})/2, & \epsilon_{fw} &= (\epsilon_{ff}\epsilon_{ww})^{1/2}. \end{aligned}$$

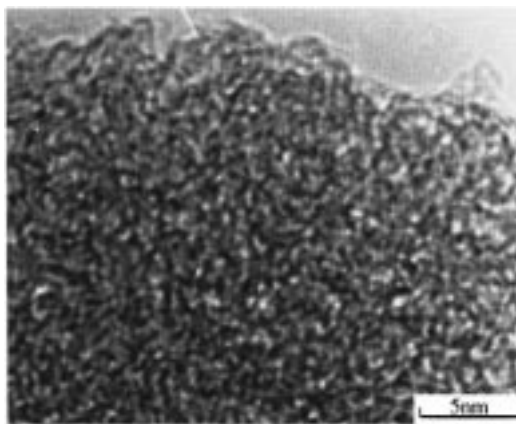


FIG. 1. TEM of a pitch-based activated carbon fiber. White areas are pores, gray areas are pore walls, dark areas are thicker pore walls. From Ref. 33.

Here, the σ 's and ϵ 's are the size and energy parameters in the LJ potential, the subscripts f and w denote fluid and wall, respectively, z is the coordinate perpendicular to the pore walls, and k_B is the Boltzmann's constant. For a given pore width H , the total potential energy from both walls is given by,

$$\phi_{\text{pore}}(z) = \phi_{fw}(z) + \phi_{fw}(H-z). \quad (3)$$

We define H to be the distance separating the planes through the centers of the carbon atoms in the first layer of the opposing walls.

Figure 1 shows a TEM image of a pitch-based activated carbon fiber. Characterization methods based on nitrogen adsorption have been used to determine the pore size distribution in these samples.³⁰ The maximum deviation in the pore width was within 10% of the mean pore width. Since the porous matrix is formed from the interstices created by re-orientation of the basal graphitic planes during the activation process,³⁴ a regular slit shaped geometry is a reasonable first approximation in modeling these porous materials. We expect the approximation of a structureless graphite wall to be a good one in our present study, since the diameter of the LJ CCl₄ molecule (0.514 nm) is much larger than the C–C bond length in graphite (0.14 nm), so that the CCl₄ molecules only feel a mild corrugation in the fluid–wall potential in passing along the surface. This has been confirmed by simulations of monolayers of methane on structured, planar carbon walls,³⁵ where wall structure had only a minor effect for temperatures down to 60 K, and by Miyahara and Gubbins,²¹ where it was found that the structure of methane was practically identical when confined between smooth and structured graphite pore walls, for both the fluid as well as the solid phase.

The simulation runs were performed in the grand canonical ensemble as described in Ref. 36, fixing the chemical potential μ , the volume V of the pore and the temperature T . The pore width in the simulation was varied from $2\sigma_{ff}$ to $15\sigma_{ff}$ accommodating single adsorbed layers to up to 14 confined layers of CCl₄ (see Table I), and the rectilinear simulation cell was $10\sigma_{ff}$ by $10\sigma_{ff}$ in the plane parallel to the pore walls, consistent with a cutoff of $5\sigma_{ff}$ for the fluid–fluid interaction. The system typically had up to 200–1200 particles, and periodic boundary conditions were employed in

the plane parallel to the pore walls. The simulation was setup such that insertion, deletion, and displacement moves were attempted with equal probability, and the displacement step was adjusted to have a 50% probability of acceptance. Thermodynamic properties were averaged over 100–500 million individual Monte Carlo steps. The length of the simulation was adjusted such that a minimum of 50 times the average number of particles in the system would be inserted and deleted during a single simulation run.

The free energy formalism used here (see Sec. II B 2) is quite general; it is not necessary to assume any type of crystalline structure in advance. Thus, for the sake of generality and simplicity, a rectilinear simulation cell was chosen as opposed to a geometry that is consistent with a particular structure of the confined solid phase. In order to avoid artifacts in the phase behavior due to small system size and incommensurable nature of the crystalline phase at the edges of the simulation cell, we performed a system size scaling study, and chose cell dimension to be large enough for the edge effects to be negligible (see Appendix B).⁴¹ The conclusion of this system size study is similar to that of a similar system size study for bulk systems by Lynden-Bell *et al.*²⁹

2. Free energy method

The method relies on the calculation of the Landau free energy as a function of an effective bond orientational order parameter Φ , using GCMC simulations. The Landau free energy is defined by²⁷

$$\Lambda[\Phi] = -k_B T \ln(P[\Phi]) + \text{constant}, \quad (4)$$

where $P[\Phi]$ is the probability of observing the system having an order parameter value between Φ and $\Phi + \delta\Phi$. The probability distribution function $P[\Phi]$ is calculated in a GCMC simulation by collecting statistics of the number of occurrences of a particular value of Φ in the form of a histogram, with the help of umbrella sampling.³⁷ For a particular phase, for instance phase A, the grand free energy Ω_A is related to the Landau free energy by

$$\exp(-\beta\Omega_A) = \int_{\Phi_{\min,A}}^{\Phi_{\max,A}} d\Phi \exp(-\beta\Lambda[\Phi]). \quad (5)$$

The grand free energy at a particular temperature can be calculated by numerically integrating over the order parameter range ($\Phi_{\min,A}$ to $\Phi_{\max,A}$) that corresponds to the particular phase A in consideration. More complete details of the method for confined systems are given elsewhere.^{25,28,29}

We use a two-dimensional order parameter previously introduced by Mermin³⁸ to characterize the order in each of the molecular layers,

$$\Phi_j = \left| \frac{1}{N_b} \sum_{k=1}^{N_b} \exp(i6\theta_k) \right| = |\langle \exp(i6\theta_k) \rangle_j|. \quad (6)$$

Φ_j measures the hexagonal bond order within each layer j . Nearest neighbors in the same layer of a given molecule were identified as those molecules that were less than a cutoff distance r_{nn} away. We used a cutoff distance $r_{nn} = 1.3\sigma_{ff}$, corresponding to the first minimum in the $g(r)$ function. Each nearest neighbor bond has a particular orien-

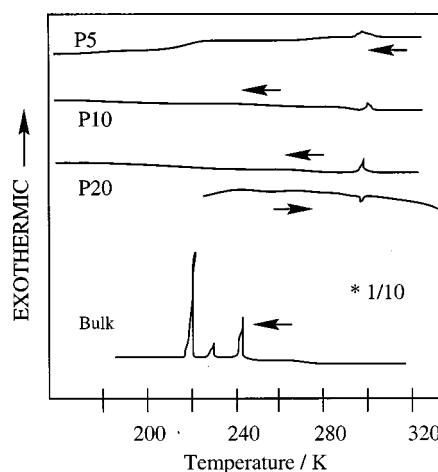


FIG. 2. DSC scans for freezing of CCl_4 in the bulk and melting/freezing of CCl_4 confined in ACF's, after subtraction of background signal. Each scan is shifted in vertical scale for the sake of clarity. The scale for the bulk is reduced by a factor of 10. The arrows represent the direction of the temperature scan, i.e., freezing or melting; DSC scan corresponding to a melting run is shown only for the case of P20 ACF.

tation in the plane of the given layer, with respect to a reference axis, and is described by the polar coordinate θ . The index k runs over the total number of nearest neighbor bonds N_b in layer j . The overall order parameter Φ is an average of the hexagonal order in all the layers,

$$\Phi = \left(\sum_{j=1}^{N_{\text{layers}}} \Phi_j \right) / N_{\text{layers}}. \quad (7)$$

For molecules with isotropic interaction potential the only two-dimensional closed packed structure is the hexagonal crystal. The quantity Φ is invariant under rotation about the z axis. We expect $\Phi = 0$ when all the layers have the structure of a two-dimensional liquid, $\Phi = 1$ in the solid phase and $0 < \Phi < 1$ in the orientationally ordered phase.

III. RESULTS

A. Experiment

In Fig. 2 is shown the evolution in the DSC patterns of different CCl_4 -ACF samples obtained during melting and freezing runs. The positions of the peaks in the DSC spectrum were found to be independent of the temperature scanning rate in the range 1.0–5.0 K min^{-1} . The scan for bulk CCl_4 is shown as a reference; three ‘‘exothermic’’ peaks at 242 K, 228 K, and 218 K are observed during the freezing run, and correspond to liquid to metastable fcc–solid phase, fcc to rhombohedral phase, and rhombohedral to monoclinic phase, respectively. The observed transitions are systematically shifted by 10 K compared to the values found in the literature because of supercooling achieved during the freezing run. Freezing/melting in the confined system occurs at 299 K; the peak positions in each of the DSC scans for melting and freezing runs corresponding to CCl_4 confined in ACF's (P5, P10, and P20) show an *upward* temperature shift of 57 K. Unlike the prediction by the Gibbs–Thomson equation, the freezing temperature is found to be independent of pore width in the micropore regime ($H = 1.0$ – 1.4 nm); see

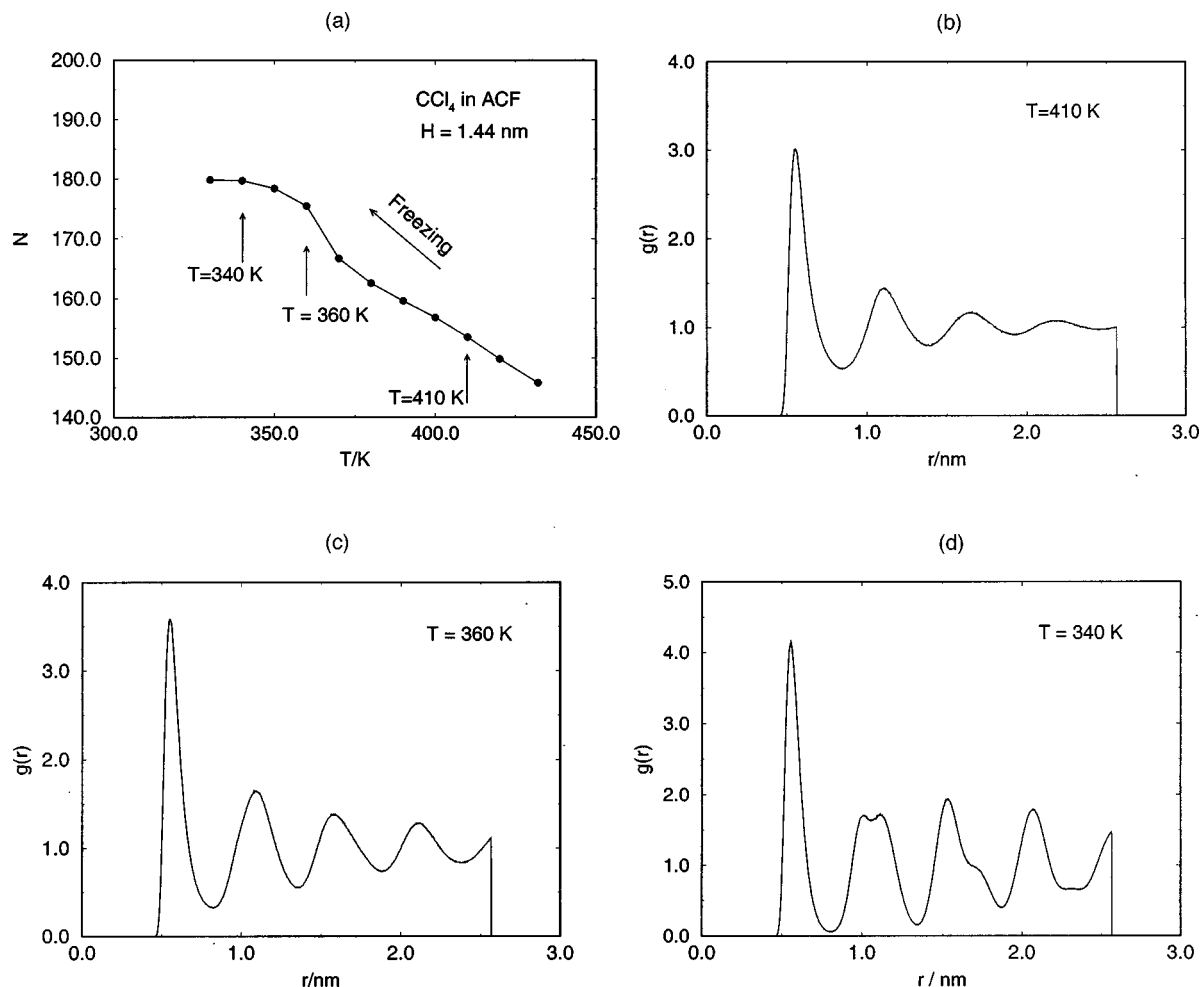


FIG. 3. Molecular simulation results showing amount of adsorption during a freezing run and structure of confined LJ CCl_4 in a graphite pore of width $H = 1.44$ nm. Bulk gas phase is at 1 atm pressure. The confined phase has two molecular layers of CCl_4 . The pair correlation functions in (b) and (c) represent an isotropic fluidlike phase, while the $g(r)$ in (d) corresponds to a hexagonal crystal.

Fig. 8. The enthalpies of freezing for the confined system, calculated from the peak areas were reproducible to within 1.0%, and were much less than that of the bulk.³⁰ A similar trend in the shift in freezing temperature was also observed for the case of benzene confined in ACF fibers.³⁹ The nature of the solid phase cannot be determined by DSC experiments alone. However, the peaks corresponding to the solid–solid transitions that take place in the bulk are absent in the confined system.

B. Simulation

The adsorption of CCl_4 in the carbon slit pores of various pore widths was calculated as a function of temperature, as the system was cooled. The chemical potential of CCl_4 in the GCMC simulation was always maintained at a value corresponding to an external bulk pressure of 1 atm. A Lennard-Jones equation of state was used to relate the chemical potential to the pressure.⁴⁰ For a pore width $H = 1.44$ nm (modeled after P20 ACF), the adsorption curve is shown in Fig. 3 along with pair correlation functions at three different temperatures. The confined phase is characterized by two layers (see Table I). The $g(r)$ plots represent the in-plane two-dimensional pair correlation functions within each layer.

A sharp increase in the adsorption is seen to occur on cooling from 380 K to 360 K, and the corresponding pair correlation functions (at 410 K and 360 K) show that this jump is not due to a freezing transition, as the structure of the fluid remains isotropic even at 360 K. However, comparing the rates of decay of $g(r)$ with r , the positional correlations at 360 K are longer ranged than those at 410 K. Since the system is close to the two-dimensional limit, there is the possibility of an orientationally ordered phase intervening between the disordered liquid phase and the positionally ordered crystal phase; such a phase could cause the jump in the adsorption curve (see Appendix A). The pair correlation function at 340 K represents a 2D hexagonal crystal phase.

In Fig. 4 is shown the heat capacity of the system as well as the order parameter Φ as a function of temperature. The peak in the heat capacity occurs simultaneously with a jump in the orientational order parameter Φ , in a temperature range where the positional correlations show no long range order [the $g(r)$ functions remain isotropic]. The heat capacity peak and the jump in the orientational order parameter are reminiscent of the nonuniversal behavior predicted by the transition from the liquid to an orientationally ordered phase (see Appendix A) that occurs at the same temperature at

which the jump in the adsorption curve is seen. Further evidence of such a transition was provided by studying the defect structures; isolated and bound disclination pairs were observed in the snapshots of the simulation.²⁵

The Landau free energy was calculated as a function of the average hexagonal bond order Φ for different temperatures for CCl_4 confined in the graphite pore of width, $H = 1.44$ nm. Each Landau free energy curve at a particular temperature possessed three minima, corresponding to three phases in the system; a liquid phase “L” with $\Phi \approx 0$ and $g(r)$ similar to Fig. 3(b), an orientationally ordered hexatic phase “I” with $0 < \Phi < 0.85$ and $g(r)$ similar to Fig. 3(c), and a hexagonal crystal phase “C” with $\Phi \approx 0.85$ and $g(r)$ similar to Fig. 3(d). The grand free energy was calculated from the Landau free energy curves using Eq. (5). The grand free energy Ω as a function of temperature for the three phases is shown in Fig. 5. The weak crossover of the “L” and the “I” branches represents a transition to the hexatic phase at $T = 355$ K (see Appendix B). The freezing transition occurs at $T = 342$ K.

The Landau free energy calculation was repeated for the different pore sizes described in Table I. For pore widths that accommodate one to three confined CCl_4 layers, it was found that all the layers froze in unison at the freezing temperature, and that this temperature was much higher than the bulk freezing temperature of LJ CCl_4 . For pore widths that accommodate four or more layers of adsorbate, an orientationally ordered phase was again observed.²⁵ However, for these larger pore widths, it was found that the contact layers froze at a higher temperature than the inner layers which in turn froze at a temperature above the bulk freezing temperature. The Landau free energy formulation provided the means of calculating both transition temperatures. Each Landau free energy curve at a particular temperature showed a triple-well structure (with three minima), corresponding to (1) a phase with isotropic fluid structure within each layer, (2) a phase with frozen contact layer (the inner layers being fluidlike), and (3) a phase with all the layers having the structure of a 2D hexagonal crystal. The crossover of the grand free energy functions for each phase gave the thermodynamic freezing temperature of the contact layers and the inner layers. The effects of system size on the free energy results are discussed in Appendix B. The freezing temperatures of the contact and the inner layers are summarized in Table III for the various pore widths used in this study.

The parameter d in Table III, represents the interlayer distance (average distance between the confined layers of CCl_4), which depends on the pore width H ; for a given H , d is the same for the liquid and solid phases. For the bulk crystal in the simulation (fcc lattice), $d = \sqrt{2}\sigma_{\text{ff}}/\sqrt{3}$. The ease with which the fluid freezes in the pore and the extent of the hysteresis loops depend crucially on the interlayer separation d , Refs. 21,25, and 42. For $d/\sigma_{\text{ff}} \geq 0.95$ the fluid freezes into a defect free crystal in our simulations, with hysteresis loops observed during adsorption and desorption spanning 2–10 K. The defects in the crystal structure increase in the range $0.90 \leq d/\sigma_{\text{ff}} \leq 0.95$, with the extent of hysteresis loops increasing to about 10–30 K and the thermodynamic freezing temperature of the inner layers decrease as d decreases. For

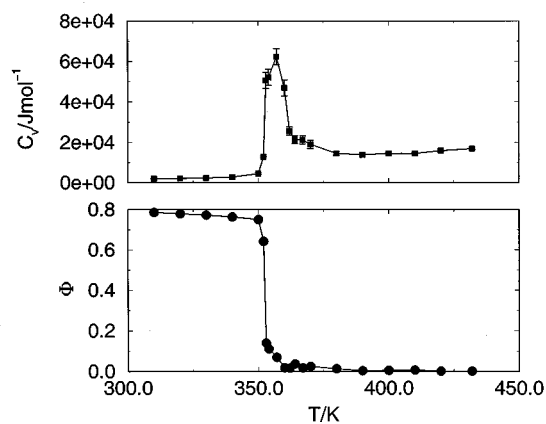


FIG. 4. Heat capacity of the whole system and the order parameter Φ as a function of temperature as the system is cooled, for the LJ CCl_4 in a graphite pore of width $H = 1.44$ nm. For this pore width the pore only contains two layers ($j = 1, 2$) and the average order parameter Φ is equal to Φ_j .

$d \leq 0.90$, the inner layers of the confined fluid *do not* undergo a freezing transition. Figure 6 shows the freezing temperature as a function of pore width for different values of d . The thermodynamic freezing temperature is not a smooth function of pore width and shows oscillatory behavior because of its crucial dependence on d . There are windows of pore widths where the fluid does not freeze because of the lower bound in the value of $d = 0.90\sigma_{\text{ff}}$ that supports freezing. However, we find that the freezing temperatures of the contact layers are only weakly dependent on d (see Table III). Thus in our study we have chosen pore widths that have different number of confined layers but all having the same interlayer separation. The variation of the freezing temperature of the contact and the inner layers as a function of pore width is shown in Fig. 7.

IV. DISCUSSION AND CONCLUSIONS

The Landau free energy formalism was used to calculate the grand free energy of the fluid and crystalline states as a function of temperature, for LJ CCl_4 confined in slit-shaped pores. The free energy difference between the ordered and the disordered state is directly calculated, thereby eliminating the need to numerically integrate the free energy, starting from a well characterized reference phase. Thus, unlike the methods that involve thermodynamic integration, this method is not limited to repulsive or weakly attractive fluid-wall potentials. In addition to the free energy, a quantitative estimate of the free energy barrier to nucleation is obtained, although such a quantity is sensitive to system size effects. However, the absolute value of the free energy difference is only a weak function of system size, and is estimated to an accuracy of $1k_B T$, as shown by Lynden-Bell *et al.*²⁹ The exact location of the equilibrium transition temperature by free energy calculation is an improvement over methods that use the jump in the density to locate the freezing/melting points in terms of accuracy, as it is independent of the width of the hysteresis loops, thereby allowing a direct consistency check with the Gibbs–Thomson equation, Eq. (1). A direct comparison with Eq. (1) would involve calculation of surface

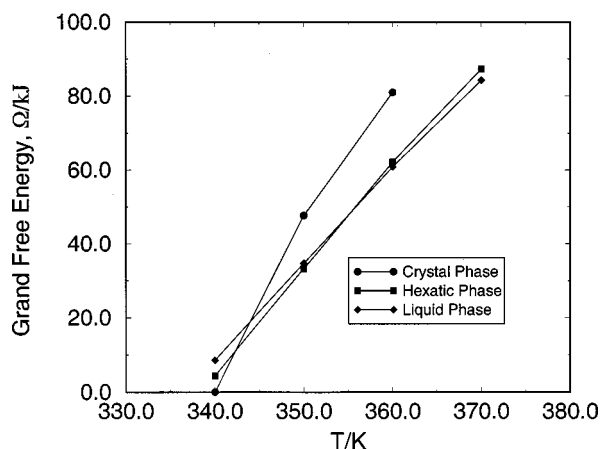


FIG. 5. The grand free energy of the three phases *L*, *I*, and *C*, as a function of temperature for LJ CCl_4 in a graphite pore of width $H=1.44$ nm. The crossover points correspond to first order phase transitions.

tensions in the simulation, which we have not attempted in this study. The behavior of ΔT vs $1/H$ in Fig. 8 is linear in the mesopore range, down to a pore width of 2.44 nm, below which there is a cross over to a “plateau” regime (in the micropore range). The plateau regime spans pore widths that can accommodate 2–3 layers of CCl_4 . For pore widths that support only a single layer of CCl_4 a sharp increase in the freezing temperature is seen. The linear regime in the mesoporous range is consistent with the Gibbs–Thomson equation. The deviation from linearity (in the micropore region) is also expected, as the Gibbs–Thomson equation breaks down in this limit (see Sec. I), for reasons that are discussed below.

There are either two or three condensed phases of confined CCl_4 , depending on the pore width. For pore widths that accommodate four or more layers, there are three phases; phase A corresponds to all layers having a liquidlike structure; phase B corresponds to the contact layers (the layers adjacent to the two pore walls) being frozen and the rest of the layers being fluidlike; phase C corresponds to all the layers being frozen. Thus, the contact layers freeze at a higher temperature than the inner layers. For pore widths that accommodate three layers or less, there are just two condensed phases, liquid and crystal, i.e., the contact layers

TABLE III. Freezing temperatures of Confined CCl_4 .

Pore width	No. of layers	T_f /K (contact layers)	T_f /K (inner layers)	d/σ_{ff}
0.94	1	410.0	...	0.95
1.44	2	342.0	...	0.95
1.74	3	335.0	...	0.84
1.93	3	333.0	333.0	0.95
2.44	4	320.0	305.0	0.95
2.76	5	310.0	273.0	0.90
2.93	5	310.0	280.0	0.95
3.68	7	300.0	248.0	0.90
3.87	7	300.0	260.0	0.95
7.25	14	290.0	254.0	0.95
bulk	∞	...	250.0	0.82

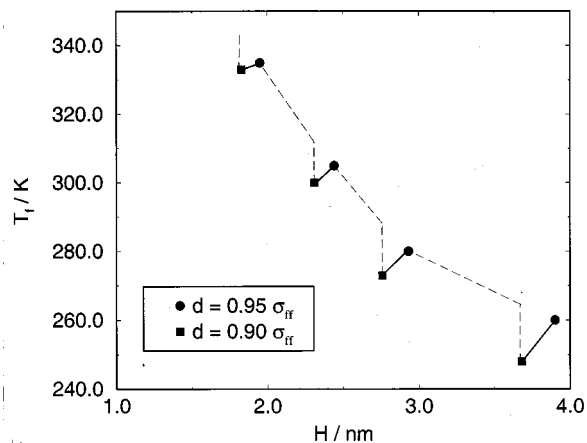


FIG. 6. The thermodynamic freezing temperature of the inner layers calculated using the Landau free energy method for different pore widths and different values of d .

freeze at the same temperature as the inner layers. It is evident from Fig. 7 that the Gibbs–Thomson equation is valid when the effect of the contact layers are negligible on the inner layers, i.e., for pores that accommodate seven molecular layers of CCl_4 or more. When the number of inner layers are comparable with the number of contact layers, a deviation from linear behavior (G–T regime) is observed, followed by a crossover to the plateau regime. It is also evident from Fig. 7 that the freezing temperature in the plateau regime is determined by the freezing of the contact layers. This region is spanned by pore widths that accommodate two to three layers of CCl_4 . Based on energetic considerations alone, it is reasonable to assume that the contact layer freezing temperature is approximately independent of H in this limit (Fig. 9); the depths of the potential well in which the contact layers are confined are approximately equal for all pore widths that support more than one layer. As the number of inner layers increase, the effective fluid–fluid potential between layers as well as entropic effects have to be taken into consideration, which is why there is a deviation from the plateau regime; the deviation from the plateau regime is ob-

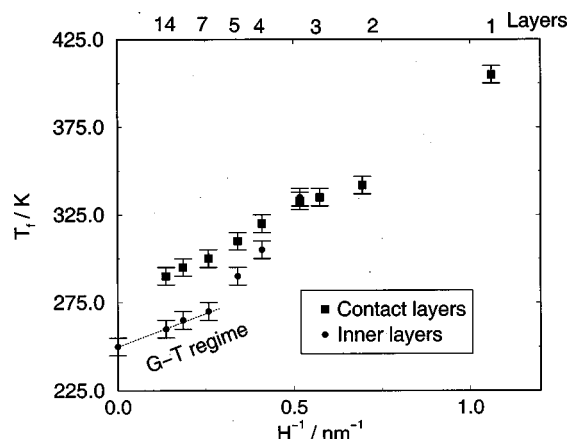


FIG. 7. Freezing of the contact and the inner layers of LJ CCl_4 as a function of pore width. The dashed line represents the region in which a linear equation is valid, consistent with the Gibbs–Thomson equation. The freezing temperatures are determined using the Landau free energy method.

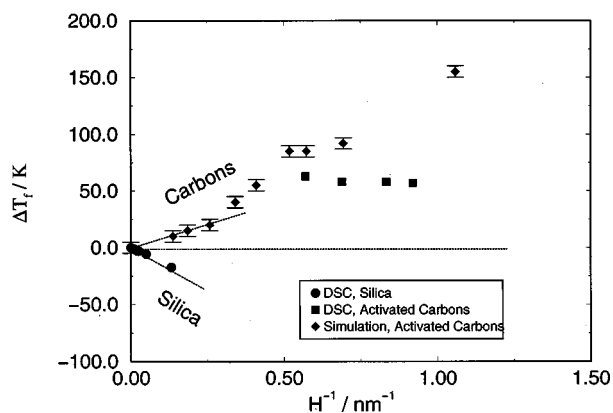


FIG. 8. Comparison of the freezing temperatures from simulation and experiment. The results for activated carbons are from this study. The DSC results for silica are reproduced from Ref. 17.

served for the contact layers as well as the inner layers. For pore widths that are small enough to accommodate just a single layer of CCl_4 , an increase in the freezing temperature is again observed as a consequence of the much deeper fluid-wall potential well (see point for smallest pore width in Fig. 8).

The comparison of the DSC results and the simulation (Fig. 8) shows that the simplified model of spherical LJ CCl_4 and regular slit shaped graphite pore with smooth walls captures the plateau in the $\Delta T(H)$ function; however it overestimates the shift in the freezing temperature. In this regime, ΔT_f is 60 K in the experiments (Fig. 2) and is about 90 K in the simulation. We note that the DSC experiments were at done at a constant pressure equal to the saturated pressure of CCl_4 at 303 K (0.15 atm), while the pressure in the simulations was set at 1 atm. This difference in the pressure is expected to have a very small effect on the freezing temperature²¹ (the solid-fluid coexistence line in the P-T phase diagrams have a slope nearly equal to infinity). We recalculated the freezing temperatures in our simulations for the pressure used in the DSC experiments and found the difference to be less than 2%. It is difficult to see the cross-over behavior in experiments, due to the lack of availability of well characterized graphitic pores in the mesopore region. The overestimation of the freezing temperature shift in the simulation is a reflection of the simplicity of the model used. It is easier for spherical molecules in slit pores to freeze when compared to five-site LJ tetrahedral molecules (a more realistic representation of CCl_4) in a real activated carbon. The confined crystal phase has perfect in-plane bond orientational order within each layer and, in addition requires that the phase of the complex order parameter Φ_j within each layer j be the same. It is intuitively clear that both the in-plane ordering and the phase ordering of the layers are easier with spheres compared to tetrahedrons. More realistic fluid-fluid potential models based on site-site LJ interactions^{43,44} could lead to an improvement in the prediction of the simulation results.

Another simplifying assumption in our simulation is the slit shaped geometry to represent the ACF. The electron micrograph of graphitic pores in Fig. 1 points to the need to

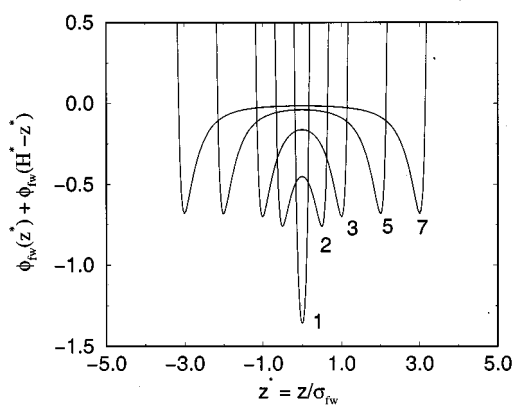


FIG. 9. Plot showing the reduced fluid wall potential energy as a function of position perpendicular to the pore wall for different pore widths accommodating 1,2,3,5, and 7 confined layers.

include important features like networking, polydispersity, surface corrugation, and irregularities and pore bottlenecks that are ignored in our model;⁴⁵ these features are bound to deter the freezing transition in real porous materials. The typical pore size distribution in activated carbon fibers is about 10% around the mean pore size of the sample, and there is a distribution of parallel slit shaped pores and pores having a wedge geometry. In addition, the presence of active sites (for example, NH_2 , $\text{CH}=\text{O}$, and CH_3OH) on the adsorbent surface have a strong influence on the freezing of confined fluids, causing a depression in the freezing temperature.⁴⁶ The absence of some of these features in our simulations could possibly account for the over estimation of the shift in the freezing temperature.

Kaneko *et al.* have reported the enthalpy change on freezing in ACF based on the DSC scans that are much lower than the enthalpy change in the bulk.³⁰ Based on our simulation results there can be more than one reason for freezing in confined systems being weakly first order. Thus, the enthalpy change in the transition from the orientationally ordered phase to the crystal phase can be considerably reduced when compared with the bulk. The heat capacity plot in Fig. 4 shows a peak corresponding to the orientational ordering (hexatic phase) of the confined liquid. It is clear that most of the entropy change occurs during this transition, and as a result, the orientationally ordered fluid to crystal phase is weakly first order. Iiyama *et al.*^{47,48} employed x-ray diffraction to study the structure of confined CCl_4 in ACF. The authors found extended positional correlations in the confined liquid phase providing indirect experimental evidence of the possibility of an orientationally ordered phase. The orientational ordering transition is not captured in the DSC scans in Fig. 2, possibly because the real porous material has corrugations in the fluid-wall potential, due to the crystal structure of graphite, that makes it periodic. This periodicity in the wall potential exerts a hexatic field, that favors the formation of the orientationally ordered phase, so that such a transition actually occurs at a higher temperature in real materials as compared to simulations that use a smooth wall potential. One possibility is that such a peak is present at temperatures higher than the DSC scans in Fig. 2. However,

it is also possible that this orientational ordering occurs at a temperature higher than the layering transition temperature, in which case such a peak would be totally absent.

Polydispersity in the real porous material can also account for the low values of the observed enthalpy change. The pore size distribution could be such that a large fraction of the pores have a pore width such that the inter layer distance in the confined phase is less than the lower bound for d that supports freezing. Thus only a small fraction of the pores actually support a crystal phase which may cause an underestimation of the value of the enthalpy of freezing. Curry *et al.*⁴⁹ studied the freezing of simple fluids in a corrugated pore model that consisted of a slit pore with rectangular grooves carved out of one of the surfaces. Over a range of groove depths, the confined phase consisted of fluid and solid portions in equilibrium, i.e., fluid filled nanocapillaries separated by solid strips, supporting the above theory. Experiments that measure the structure factor in the confined phase using x-ray scattering could shed more light on this speculation. If this is indeed the case one would observe significant liquidlike structure even below the freezing temperature of the confined CCl_4 .

ACKNOWLEDGMENTS

It is a pleasure to thank M. Sliwiska-Bartkowiak for helpful discussions. This work was supported by grants from the National Science Foundation (Grant No. CTS-9896195) and grant-in-aid for Scientific Research (09243102, priority area 288, Japan). The computational facilities were provided in part by the San Diego Super Computer Center under a NSF/NPACI grant (No. MCA93S011P).

APPENDIX A

Two-dimensional systems have a special significance for phase transitions in which continuous symmetry is broken (such as freezing transitions). The Mermin–Wagner theorem⁵⁰ states that long range order (LRO) cannot exist in such systems. Halperin and Nelson proposed the “KTHNY” mechanism for melting of a crystal in two dimensions⁵¹ which involves two transitions of the Kosterlitz–Thouless (KT) type.⁵² The first is a transition between the crystal phase (having positional quasi-LRO and orientational LRO) and a hexatic phase (having positional disorder and orientational quasi-LRO); the second transition is between the hexatic phase and the liquid phase (having positional and orientational disorder). A quasi-long range ordered phase is characterized by an algebraic decay of the two point correlation function associated with the order parameter as opposed to an exponential decay in the disordered phase. The crystal to hexatic transition occurs through the unbinding of dislocation pairs, and the hexatic to liquid transition involves the unbinding of disclination pairs. Each KT transition is accompanied by a nonuniversal peak in the specific heat above the transition temperature, associated with the entropy liberated by the unbinding of the vortex pairs. The spontaneous ordering of the adsorbed molecules in the graphite pore into distinct two-dimensional layers makes it a quasi-two-dimensional system. Extensive simulation results of strictly

two-dimensional systems have failed to provide compelling evidence to support the KTHNY melting scenario (for example, see Ref. 53). However a recent study by Zangi and Rice⁵⁴ has cast some light on the role of the *out-of-plane* motion (as in the case of a quasi-two-dimensional system as opposed to a strictly two-dimensional system) in the occurrence of an intervening orientationally ordered phase.

APPENDIX B

The free energy results suggest that the orientational ordering transition is weakly first order (crossing over of the free energy curves for “L” and “I” phases). In order to show that this transition remains first order in the thermodynamic limit, a finite size scaling analysis is required. A continuous transition can look like a weakly first order transition in a finite system. The reason for this is that there is always a nonzero probability of observing the unstable phase because of interface and boundary effects in a finite system, that is proportional to

$$\exp(-\beta N \delta f), \quad (\text{B1})$$

where δf is the difference in intrinsic free energy between the two phases. In the thermodynamic limit, this probability vanishes. The system size scaling study for the model used here,⁴¹ showed that the structure of the hexatic phase (phase “I”) was sensitive to the linear dimensions of the simulation cell parallel to the plane of the pore walls, L_{cell} , for $L_{\text{cell}} < 15\sigma_{\text{ff}}$. However according to the Landau free energy results, the location of the thermodynamic freezing temperature was independent of system size for $L_{\text{cell}} \geq 10\sigma_{\text{ff}}$. The absolute free energy differences between phases were independent of system size; however, the height of the nucleation barrier showed a strong dependence on system size. The snapshots of molecular configurations in the confined crystalline phase, showed no evidence of defect structures at the simulation cell boundaries,²⁵ thus a cell size of $L_{\text{cell}} = 10\sigma_{\text{ff}}$ is large enough not to introduce artifacts in the freezing behavior due to finite system size.

¹C. Eyraud, J. F. Quinson, and M. Brun, in *Characterization of Porous Solids*, edited by K. Unger, J. Rouquerol, K. S. W. Sing, and H. Kral (Elsevier, Amsterdam, 1988), p. 307.

²J. Warnock, D. D. Awschalom, and M. W. Shafer, *Phys. Rev. Lett.* **57**, 1753 (1986).

³J. L. Tell, H. J. Maris, and G. M. Seidel, *Phys. Rev. B* **28**, 5122 (1983).

⁴R. H. Torii, H. J. Maris, and G. M. Seidel, *Phys. Rev. B* **41**, 7167 (1990).

⁵P. E. Sokol, W. J. Ma, K. E. Herwig, W. M. Snow, Y. Wang, J. Koplik, and J. R. Banavar, *Appl. Phys. Lett.* **61**, 777 (1992).

⁶J. H. Strange, M. Rahman, and E. G. Smith, *Phys. Rev. Lett.* **71**, 3589 (1993).

⁷E. Molz, A. P. Y. Wong, M. H. W. Chan, and J. R. Beamish, *Phys. Rev. B* **48**, 5741 (1993).

⁸K. M. Unruh, T. E. Huber, and C. A. Huber, *Phys. Rev. B* **48**, 9021 (1993).

⁹J. A. Duffy, N. J. Wilkinson, H. M. Fretwell, A. A. Alam, and R. Evans, *J. Phys.: Condens. Matter* **7**, L713 (1995).

¹⁰E. W. Hansen, M. Stöker, and R. Schmidt, *J. Phys. Chem.* **100**, 2195 (1996).

¹¹K. J. Elder, P. A. Reynolds, F. Trouw, and J. W. White, *J. Chem. Soc. Chem. Commun.* **1996**, 155 (1996).

¹²J. Krim, J. P. Coulomb, and J. Bouzidi, *Phys. Rev. Lett.* **58**, 583 (1987).

¹³K. Morishige and K. Nobuoka, *J. Chem. Phys.* **107**, 6965 (1997).

¹⁴K. Morishige and K. Kawano, *J. Chem. Phys.* **110**, 4867 (1998).

¹⁵K. Overloop and L. Van Gerven, *J. Magn. Reson., Ser. A* **101**, 179 (1993).

- ¹⁶H. F. Booth and J. H. Strange, *Mol. Phys.* **93**, 263 (1998).
- ¹⁷M. Sliwinski-Bartkowiak, J. Gras, R. Sikorski, R. Radhakrishnan, L. D. Gelb, and K. E. Gubbins, *Langmuir* **15**, 6060 (1999).
- ¹⁸R. Evans and U. Marini Betello Marconi, *J. Chem. Phys.* **86**, 7138 (1987).
- ¹⁹A. Chelkowski, *Dielectric Physics* (Elsevier, North-Holland, New York, 1980).
- ²⁰P. Debye, *Polar Molecules* (Chemical Catalog, New York, 1929).
- ²¹M. Miyahara and K. E. Gubbins, *J. Chem. Phys.* **106**, 2865 (1997).
- ²²M. Maddox and K. E. Gubbins, *J. Chem. Phys.* **107**, 9659 (1997).
- ²³T. Suzuki, K. Kaneko, and K. E. Gubbins, *Langmuir* **13**, 2545 (1997).
- ²⁴H. Dominguez, M. P. Allen, and R. Evans, *Mol. Phys.* **96**, 209 (1999).
- ²⁵R. Radhakrishnan and K. E. Gubbins, *Mol. Phys.* **96**, 1249 (1999).
- ²⁶D. Frenkel and A. J. C. Ladd, *J. Chem. Phys.* **81**, 3188 (1984).
- ²⁷L. D. Landau and E. M. Lifshitz, *Statistical Physics*, 3rd ed. (Pergamon, London, 1980).
- ²⁸J. S. Van Duijneveldt and D. Frenkel, *J. Chem. Phys.* **96**, 4655 (1992).
- ²⁹R. M. Lynden-Bell, J. S. Van Duijneveldt, and D. Frenkel, *Mol. Phys.* **80**, 801 (1993).
- ³⁰K. Kaneko, A. Watanabe, T. Iiyama, R. Radhakrishnan, and K. E. Gubbins, *J. Phys. Chem.* **103**, 7061 (1999).
- ³¹W. A. Steele, *Surf. Sci.* **36**, 317 (1973).
- ³²W. A. Steele, *The Interaction of Gases with Solid Surfaces* (Pergamon, Oxford, 1974).
- ³³K. Oshida and M. Endo (private communication, 1998).
- ³⁴R. C. Bansal, J. P. Donnet, and F. Stoeckli, *Active Carbon* (Marcel Dekker, New York, 1988), Chap. 1.
- ³⁵S. Jiang and K. E. Gubbins, *Mol. Phys.* **80**, 103 (1993).
- ³⁶G. B. Woods and J. S. Rowlinson, *J. Chem. Soc., Faraday Trans. 2* **85**, 756 (1989).
- ³⁷G. M. Torrie and J. P. Valleau, *Chem. Phys. Lett.* **28**, 578 (1974).
- ³⁸N. D. Mermin, *Phys. Rev.* **176**, 250 (1968).
- ³⁹A. Watanabe and K. Kaneko, *Chem. Phys. Lett.* (in press).
- ⁴⁰J. K. Johnson, J. A. Zollweg, and K. E. Gubbins, *Mol. Phys.* **78**, 3 (1993); **78**, 591 (1993).
- ⁴¹R. Radhakrishnan and K. E. Gubbins, 1999 (preprint).
- ⁴²C. L. Rhykerd, M. Schoen, D. J. Diestler, and J. H. Cushman, *Nature* **330**, 461 (1987).
- ⁴³L. S. Bartell and J. Chen, *J. Phys. Chem.* **96**, 8801 (1992).
- ⁴⁴W. L. Jorgensen and J. Tirado-Rives, *J. Am. Chem. Soc.* **110**, 3469 (1988).
- ⁴⁵K. Kaneko, C. Ishii, H. Kanoh, Y. Hanzawa, N. Setoyama, and T. Suzuki, *Adv. Colloid Interface Sci.* **76–77**, 295 (1998).
- ⁴⁶A. Vishnyakov, E. M. Piotrovskaya, and E. N. Brodskaya, *Adsorption* **4**, 207 (1998).
- ⁴⁷T. Iiyama, K. Nishikawa, T. Otowa, and K. Kaneko, *J. Phys. Chem.* **99**, 10075 (1995).
- ⁴⁸T. Iiyama, K. Nishikawa, T. Suzuki, and K. Kaneko, *Chem. Phys. Lett.* **274**, 152 (1997).
- ⁴⁹J. E. Curry, F. Zhang, J. H. Cushman, M. Schoen, and D. J. Diestler, *J. Chem. Phys.* **101**, 10824 (1994).
- ⁵⁰N. D. Mermin and H. Wagner, *Phys. Rev. Lett.* **17**, 1133 (1966).
- ⁵¹B. I. Halperin and D. R. Nelson, *Phys. Rev. Lett.* **41**, 121 (1979); D. R. Nelson and B. I. Halperin, *Phys. Rev. B* **19**, 2457 (1979); A. P. Young, *ibid.* **19**, 1855 (1979).
- ⁵²J. M. Kosterlitz and D. J. Thouless, *J. Phys. C* **5**, L124 (1972); **6**, 1181 (1973).
- ⁵³P. Bladon and D. Frenkel, *Phys. Rev. Lett.* **74**, 2519 (1995).
- ⁵⁴R. Zangi and S. A. Rice, *Phys. Rev. E* **58**, 7529 (1998).